RSC Advances

Graphic TOC

Title: High strength biocompatible PEG single-network hydrogels

Authors: Shan Shan Qian, Chao Zhou, Li Qun Xu, Cen Lian*, Fang Yao, Guo Dong Fu*

Single-chain PEG hydrogel with extremely high strength were prepared via a precise design and control over the molecular topology of the polymeric network.
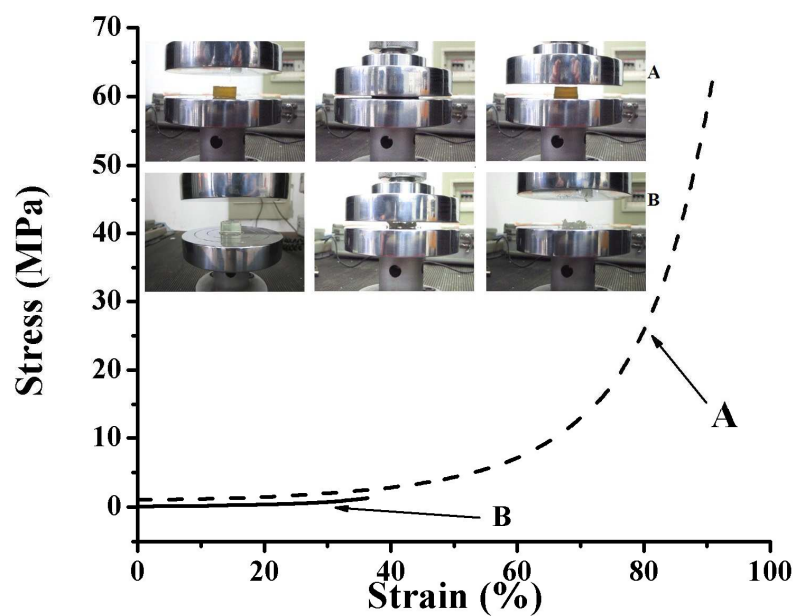
High strength biocompatible PEG single-network hydrogels

ShanShan Qian[1], Chao Zhou[1], LiQun Xu[1], Fang Yao[1], Lian Cen[2,3]*, GuoDong Fu[1]*

[1]School of Chemistry and Chemical Engineering, Southeast University

Jiangning District, Nanjing, Jiangsu Province, P.R. China 211189

[2]School of Chemical Engineering, East China University of Science and Technology,

No.130, Mei Long Road, Shanghai, P.R. China 200237;

[3]National Tissue Engineering Center of China,

No.68, East Jiang Chuan Road, Shanghai, P.R. China 200241.

* To whom correspondence should be addressed**:**

Tel.: +86-25-52090625; Fax: +86-25-52090625

Email: fu7352@seu.edu.cn; cenlian@hotmail.com

Abstract

In this work, PEG-based single-chain hydrogels with extremely high strength were successfully prepared via a precise design and control over the molecular topology of the polymeric network. Initially, well-defined PEG macromolecules with uniformly dispersed pendant alkynyl groups $(PEG_n(C{\equiv}CH))_m$ on their main chains were synthesized via amine-epoxy chain extension reaction of α, ω-diepoxy PEG and propargylamine. The subsequent copper (I)-catalyzed azide-alkyne 1, 3-dipolar cycloaddition (CuAAC) of $(PEG_n(C{\equiv}CH))_m$ and α, ω-diazido PEG_n $(PEG_n(N_3)_2)$ gave rise to tough PEG-based hydrogels $(Gel\text{-}PEG_n(N_3)_2\text{-}(PEG_n(C{\equiv}CH))_m)$. The lattice size of the $Gel\text{-}PEG_n(N_3)_2\text{-}(PEG_n(C{\equiv}CH))_m$ networks can be tailored by varying chain lengths of PEG repeating segments in $(PEG_n(C{\equiv}CH))_m$ and $PEG_n(N_3)_2$. Different from traditional PEG hydrogels prepared by CuAAC, such as hydrogels from tetrakis (2-propynyloxymethyl) methane and $PEG_n(N_3)_2$, the current novel hydrogels possess not only a high mechanical strength up to 62.5 Mpa, but is also biodegradable favored by the presence of triethylamine groups in the $(PEG_n(C{\equiv}CH))_m$ macromolecules. Furthermore, excellent biocompatibility of the $Gel\text{-}PEG_n(N_3)_2\text{-}(PEG_n(C{\equiv}CH))_m$ was demonstrated according to the in vitro cytotoxicity assay. Hence, it can be ascertained that $Gel\text{-}PEG_n(N_3)_2\text{-}(PEG_n(C{\equiv}CH))_m$ has the promising potential as artificial medical devices or scaffolding materials for regenerative medicine.

1. Introduction

Hydrogels with soft tissue-mimicking consistency and high permeability to metabolites and nutrients have drawn more and more attention for their potential applications in various biomedical devices.[1-6] Unfortunately, the poor mechanical strength, uncontrollable molecular structure, and non-biodegradability of conventional hydrogels seriously dampen their popularity in biomedical fields, especially for purposes related to regenerative medicine.[7, 8] In the physiological condition, many tissues (such as cartilage, blood vessel, and ligament) function under a dynamic environment with severe mechanical requirements. For example, articular cartilage has to sustain a daily compression of several MPa.[9, 10] Hence, to bridge the performance gap between artificial gels and biological tissue is one of the challenges in modern gel science.[10] Many efforts have been made on increasing the mechanical strength of prepared hydrogels, including hydrogen-bonded hydrogels,[11-13] nanocomposite-sized gels,[14-18] and tetra-PEG hydrogels.[19, 20] Recently, Gong J.P et al. demonstrated the critical importance of double network (DN) structure of hydrogels prepared from various combinations of hydrophilic polymers.[21-25] The resulting hydrogels displayed extremely high mechanical strength with low coefficients of friction.[26, 27] However, tough hydrogels with single network (SN) are still preferred for their usage as biomaterials due to the feasible tailoring of their chemical compositions and functionalities.[28-31]

Poly (ethylene glycol) (PEG) is one of the most widely explored polymers, for its excellent amphiphilicity, nontoxic nature, and resistance to cell adhesion and protein adsorption.[32] Hence，PEG hydrogels were well prepared and widely used for applications in drug delivery and biomedical devices.[33-36] PEG hydrogels with extremely high strength but biodegradability are of special interests to biomedical scientists, for their potential as artificial and temporary devices to promote those targeted tissue regeneration with high mechanical requirements, such as tendon or articular cartilage as mentioned above.[37, 38]

It is well known that random crosslinking points and high defects occurrence in the molecular structure are two of main reasons hindered the preparation of tough SN

hydrogels. Therefore, in order to obtain tough SN hydrogels, the focus is to find a technology that could overcome the above deficiencies but with a precise control over the molecular topology of polymeric networks within hydrogels. [39] Click chemistry, especially copper(I)-catalyzed azide-alkyne cycloaddition (CuAAC), has been proposed as a highly effective approach for preparing three-dimensional well-defined polymeric networks due to its reaction specificity, quantitative yields and good functional group tolerance.[40] PEG hydrogels with a relatively high strength were prepared via CuAAC using tetrakis(2-propynyloxymethyl)methane (TPOM) and α, ω-diazido PEG_{45} ($PEG_{45}(N_3)_2$) as starting materials.[41] It is also agreed that the strength of polymer networks can be improved by increasing the crosslinking density in a controllable manner.[42, 43]

In this study, PEG-based hydrogel (Gel-$PEG_n(N_3)_2$-($PEG_n(C\equiv CH)$)$_m$ with extremely high strength was successfully prepared by controlling the molecular topology of PEG macromolecules via a combined amine-epoxy chain extension reaction and copper (I)-catalyzed azide-alkyne 1, 3-dipolar cycloaddition (CuAAC). For such purpose, alkynyl-pendant linear PEG_n derivatives ($PEG_n(C\equiv CH)$)$_m$ with a controllable number of alkyne groups were first synthesized as reported previously.[44] The subsequent CuAAC of ($PEG_n(C\equiv CH)$)$_m$ and α, ω-diazido PEG_n ($PEG_n(N_3)_2$) then yielded tough PEG-based hydrogels Gel-$PEG_n(N_3)_2$-($PEG_n(C\equiv CH)$)$_m$. The molecular topology of ($PEG_n(C\equiv CH)$)$_m$ can largely suppress the macroscopic defects in the polymer network, which extremely affect the strength of hydrogels. The lattice size of Gel-$PEG_n(N_3)_2$-($PEG_n(C\equiv CH)$)$_m$ networks was regulated by synthesis of ($PEG_n(C\equiv CH)$)$_m$ and $PEG_n(N_3)_2$ using PEG of different starting sizes. Of note, the tough hydrogel prepared in this work not only possessed excellent biocompatibility but was also biodegradable. The above promising features of Gel-$PEG_n(N_3)_2$-($PEG_n(C\equiv CH)$)$_m$ thus substantiate its potential for regenerative medicine.

2. Experimental Section

2.1 Materials

Poly (ethylene glycol) diglycidyl ether (M_n = 500) and epichlorohydrin (99%) were

1

purchased from Aldrich Chemical Co. and used as received. Sodium azide (NaN_3, 99%), pentaerythritol, $CuSO_4 \cdot 5H_2O$, sodium ascorbate, sodium hydride (NaH, 60%) and ammonium chloride (NH_4Cl) were all purchased from Shanghai Chemical Reagent Plant. L929 cells were obtained from the Chinese Academy of Sciences. RPMI-1640 medium, and phosphate buffered saline (PBS) were purchased from Gibco. Tetrahydrofuran (THF) was dried by refluxing over sodium benzophenone ketyl and distilled directly into reaction flasks. Propargyl bromide (J&K Scientific, 80%), propargylamine (J&K Scientific, 80%) and pentamethyldiethylenetriamine (PMDETA, J&K Scientific, 99%) were distilled before use. PEG (M_n = 1000 and 2000, Aldrich) were dried at 120 °C under reduced pressure for 4 h before usage.

2.2 Chemical Synthesis

2.2.1 Synthesis of alkynyl-pendant linear PEG_n derivatives (($PEG_n(C{\equiv}CH))_m$)

Linear PEG_n derivatives having pendant alkynyl groups were synthesized by chain extension reaction of DEP_n and propargylamine. DEP_{45} (5.0 g) and propargylamine (0.12 g) of equal moles were added into a round-bottom flask containing 5 mL of methanol, and the reaction mixture was stirred with the help of a mechanical stirrer at room temperature for 4 days. The reaction mixture was then dialyzed against deionized water for 72 h and the solvent was removed by rotary evaporation. A large excess of diethyl ether was added into the flask to precipitate out the crude PEG_n derivatives. The desired polymer, ($PEG_{45}(C{\equiv}CH))_7$, was collected by filtration and dried under reduced pressure overnight. ($PEG_{11}(C{\equiv}CH))_9$, ($PEG_{11}(C{\equiv}CH))_{18}$, ($PEG_{11}(C{\equiv}CH))_{28}$ and ($PEG_{22}(C{\equiv}CH))_{10}$ were synthesized in a similar manner to that of ($PEG_{45}(C{\equiv}CH))_7$, except that their reaction times were 3 days, 7 days, 14 days and 9 days, respectively.

2.2.2 Synthesis of PEG-based hydrogels $Gel\text{-}PEG_n(N_3)_2\text{-}(PEG_n(C{\equiv}CH))_m$ *via* CuAAC

($PEG_{45}(C{\equiv}CH))_7$ (0.30 g, 0.02 mmol), $PEG_{45}(N_3)_2$ (0.32g, 0.08mmol) and H_2O of 0.5 mL were added into a small vial. The vial was sonicated to make sure that the reactants were completely dissolved in H_2O. After the solution turned clear, sodium ascorbate (2.49 mg, 0.01 mmol) and $CuSO_4 \cdot 5H_2O$ (2.87 mg, 0.02 mmol) were added

into the above vial. The reaction mixture was degassed with N_2 for 10 min. After that, 3.46 mg (0.02 mmol) of PMDETA was added into the vial using a syringe. The vial was then put under ultrasonic agitation at room temperature. The gelation of the PEG-based hydrogel was occurred within 5 min. The reaction was then still allowed to react at room temperature without sonication for 12 h to obtain a uniform solid structure. After complete gelation, the gel was firstly immerged into an EDTA (5%) solution and then ethanol to remove the copper ions and PMDETA. Gel-PEG$_{11}$(N$_3$)$_2$-(PEG$_{11}$(C≡CH))$_9$, Gel-PEG$_{11}$(N$_3$)$_2$-(PEG$_{11}$(C≡CH))$_{18}$, Gel-PEG$_{11}$(N$_3$)$_2$-(PEG$_{11}$(C≡CH))$_{28}$, Gel-PEG$_{22}$(N$_3$)$_2$-(PEG$_{22}$(C≡CH))$_{10}$, and Gel-PEG$_{45}$(N$_3$)$_2$-(PEG$_{45}$(C≡CH))$_7$ were referred to PEG hydrogels prepared from the reaction mixtures of (PEG$_{11}$(C≡CH))$_9$ and PEG$_{11}$(N$_3$)$_2$, (PEG$_{11}$(C≡CH))$_{18}$ and PEG$_{11}$(N$_3$)$_2$, (PEG$_{11}$(C≡CH))$_{28}$ and PEG$_{11}$(N$_3$)$_2$, (PEG$_{22}$(C≡CH))$_{10}$ and PEG$_{22}$(N$_3$)$_2$ and (PEG$_{45}$(C≡CH))$_7$ and PEG$_{45}$(N$_3$)$_2$, respectively, with a same polymer volume fraction.

2.2.3 Synthesis of Gel-TPOM-PEG$_{45}$(N$_3$)$_2$ *via* CuAAC

0.3 g (0.15 mmol) of α, ω-diazido PEG$_{45}$ (PEG$_{45}$(N$_3$)$_2$), 2.1 mg (0.025 mmol) of tetrakis (2-propynyloxymethyl) methane, 8.7 mg (0.05 mmol) of PMDETA, and 1 mL of DMF were added into a small vial. After the mixture turned clear, the vial was degassed with argon for 20 min. CuBr of 3.6 mg (0.025 mmol) was quickly added into the above vial under ultrasonic agitation. The gelation point of the resulting hydrogel, Gel-TPOM-PEG$_{45}$(N$_3$)$_2$, was reached within 1 min. The reaction was still allowed to continue for 24 h to obtain a uniform solid structure. A uniform hydrogel was yielded upon removal from the vial. The gel was transferred to an EDTA (5%) solution to remove the copper ions and DMF. Finally, the gel was immersed into a large volume of deionized water to allow its swelling.

2.3 Characterization

The chemical structures of PEG derivatives were characterized by ^{1}H NMR, FT-IR and Gel Permeation Chromatography (GPC). ^{1}H NMR spectra were recorded on a Bruker ARX300 MHz spectrometer in CDCl$_3$ with tetramethylsilane as an internal standard. FT-IR spectra were recorded on a Bruker Vector 22 IR spectrometer. The sample was dispersed in a KBr pellet. Number-average molecular weights (M_n) were

measured by GPC using a Waters 1515 system equipped with two PL Mixed-C columns using THF as an eluent at a flow rate of 1.0 mL/min at 40 ºC against commercial polystyrene (PSt) standards (Waters ShodexVR). The morphology of the PEG-based hydrogels was observed on a scanning electron microscope (XL30 SEM) at an accelerating voltage of 25 kV. The mechanical properties of PEG-based hydrogels were measured on a MCR102 Modular Compact Rheometer Anton Paar. The compression testing of the hydrogel was measured on a CMT 4503 Electron Universal Testing machine. The swollen hydrogels were dried in a LGJ-10C freeze-dryer. The DSC measurements were performed under a nitrogen atmosphere on a Perkin Elmer DSC7 calorimeter. All samples were pre-heated to 120 ºC to erase the thermal history, then cooled to -70 ºC at a rate of 10 ºC /min, and further heated to 120 ºC again at a rate of 10 ºC /min. The thermal stability of the PEG-based hydrogel was determined on a thermogravimetric analyzer (TA SDT Q-600) with a temperature range of 50-550 ºC at a heating rate of 10 ºC/min under nitrogen atmosphere. For cytotoxicity evaluation, the optical density (OD 570) was measured at 570 nm with a Rayto RT-6000 ELISA analyzer.

2.4 Swelling degree

The swelling degree of PEG-based hydrogels was measured according to Equation 1. Briefly, a gel sample was dried until a constant weight was reached. The weight (Weight $_{dry\ gel}$) was then recorded. The dry hydrogel sample was immersed in deionized water and weighted at prescribed time points until the swelling equilibration was reached. Each value was the average of three separate measurements. The equilibrated value was recorded (Weight $_{swollen\ gel}$). The degree of swelling (DS) of hydrogels was calculated from Equation 1.

$$DS = [(Weight\ _{swollen\ gel} / Weight\ _{dry\ gel}) -1] \times 100\% \qquad (1)$$

2.5 Mechanical testing

Viscoelastic properties of PEG-based hydrogels were characterized by dynamic shear oscillation measurements. The rheology study of PEG-based hydrogels was performed on a rheometer with a 25 mm diameter parallel plate accessory. A series of PEG-based hydrogels were pre-formed into hydrogel disks of a same size (25 mm diameter, 10 mm thickness) and then dried for 24 h at room temperature before measurement. In particular, the dynamic storage modulus were determined over the frequency range of 0.1 < ω < 200 Hz. All of the measurements were carried out at

25 °C.

Compression tests were conducted with an electron universal testing machine (TMS CMT 4503) at around 25°C and 50% relative humidity. PEG-based hydrogels (8 mm in thickness and 20 mm in diameter) were subjected to compression tests with a 5000N load cell and a compressive strain rate of 1 mm/min.

2.6 In vitro degradation

The in vitro degradation of PEG-based hydrogels was carried out at 37 ºC in phosphate-buffered solution (PBS, pH = 7.4, 0.01M) containing sodium azide (1.0 mM) as a bacteriostatic agent. The PEG-based hydrogel of 100 mg (m_o) was immersed in a small bottle containing 20ml of the above buffered solution with gentle shaking. The buffered solution was renewed every week. The hydrogel samples were periodically removed from the buffer and washed with distilled water. Their final mass (m_t) was obtained after complete drying in a freeze-dryer. The percentage of the mass loss was calculated from Equation 2.

$$\text{Mass loss (\%)} = (m_o\text{-}m_t)/m_o \times 100\% \tag{2}$$

Where m_o is the initial dry gel mass and m_t is the gel mass after immersion into PBS solution for predetermined time periods.

2.7 MTT viability assay

The relative cytotoxicity of the prepared PEG-based hydrogels was estimated by MTT viability assay. Prior to cell culture, all gels samples were sterilized with 70% (v/v) ethanol for 72 h, and then washed thoroughly with sterile PBS to remove any residual alcohol. Five samples were placed in RPMI-1640 medium (0.1g/mL) for 72 h, respectively. The corresponding extracts were collected as respective conditioned media for subsequent cell viability tests known as the MTT-dye reduction assay using L929 cells. L929 cells were cultured in a 24-well culture plates in RPMI-1640 medium supplemented with 10% FBS, 1% L-glutamine, and 1% penicillin/streptomycin (defined as the growth medium) and then incubated at 37 ºC in 5% CO_2, 95% humidified atmosphere for 48 h. After cells reached 90% confluence, they were detached by treating with trypsin-EDTA (0.025% and 0.02%, respectively). The cell suspension was centrifuged at 1300 rpm for 10 min followed by resuspension of cell pellets with the growth medium. The prepared cell suspension was seeded into 96-well plates at 1×10^6 viable cells per well and incubated with the conditioned media for 24 h, 48 h and 72 h, respectively, at 37 ºC in 5% CO_2 before MTT assays. Cell viability was measured using MTT assay. Experimental groups, negative control and

positive control groups were cells cultured with the RPMI-1640, phenol solution, and RPMI-1640 medium, respectively. After 24 h, 48 h and 72 h treatment, 10 μL MTT (5 mg/ml) was added into each well of microplates. The plates were shaken briefly and incubated further for 4 h at 37 ℃. Then 100 μL of DMSO was added into each well to dissolve intracellular MTT formazan crystals. The absorbance (OD) was determined at 570 nm using a multifunctional microplate reader (Biotek synergy 2). Nonseeded wells treated with corresponding media were assayed as blank controls which were then subtracted from the corresponding samples. The cell relative viability of each sample was expressed as a percentage of the OD value measured from the respective sample over that of the positive control. Experiments were performed in triplicate and were repeated thrice. Data were presented as mean ± standard deviation from three separate runs, and each of them was the mean of triplicate experiments. Comparison of the cell relative viability between different groups was also carried out. Student t-tests were used to determine statistical significance between groups, and $p<0.05$ was considered significant.

3. Results and discussion

3.1 Synthesis

The schematic illustration for preparing PEG-based building blocks and PEG-based hydrogels (Gel-PEG$_n$(N$_3$)$_2$-(PEG$_n$(C≡CH))$_m$) is shown in Scheme 1. The synthetic strategy involves three main steps: i) the synthesis of α,ω-diazido PEG$_n$ (PEG$_n$(N$_3$)$_2$, n = 11, 22 and 45) via the ring-opening of α,ω-diepoxy PEG$_n$ (DEP$_n$, n = 11, 22 and 45, Supporting information); ii) well-defined PEG macromolecules with uniformly dispersed pendant alkynyl groups ((PEG$_n$(C≡CH))$_m$, n = 11, 22 and 45) via chain extension of DEP$_n$ (n = 11, 22 and 45) with propargylamine; iii) the construction of PEG-based hydrogel networks with different PEG-based building blocks via CuAAC.

The hydroxyl groups of PEG were converted to epoxy groups according to the literature.[45] A series of well-defined alkynyl-pendant linear (PEG$_n$(C≡CH))$_m$ (n = 11, 22 and 45) were synthesized via chain extension of DEP$_n$ (n = 11, 22 and 45) with propargylamine. Their molecular weight and polydispersity index (PDI) of (PEG$_n$(C≡CH))$_m$ are summerized in Table 1. The size of (PEG$_n$(C≡CH))$_m$ and the number of the alkynyl groups can be tailored by varying the relative feed ratio of

DEP$_n$ and propargylamine. Figure 1 shows the GPC traces of (PEG$_n$(C≡CH))$_m$ macromolecules using DEP$_{11}$ as starting materials. The (PEG$_{11}$(C≡CH))$_m$s with M_n of 4.9x10^{3}g/mol, 9.3x10^{3}g/mol and14.6x10^{3}g/mol were obtained. In comparison to DEP$_{11}$ which has a PDI of about 1.03, the PDI of (PEG$_n$(C≡CH))$_m$ was increased to about 1.4. The number of the alkynyl groups in (PEG$_n$(C≡CH))$_m$ can be calculate from Equation 3:

$$N = (M_{n((PEGn(C≡CH))m)})/M_{n(PEG)}+1 \tag{3}$$

As shown in Table 1, (PEG$_{11}$(C≡CH))$_m$ with alkynyl groups of 10, 19 and 29 were synthesized. (PEG$_{22}$(C≡CH))$_m$ and (PEG$_{45}$(C≡CH))$_m$ with alkynyl group of 11 and 8 were also prepared. The chemical structure of (PEG$_{45}$(C≡CH))$_7$ was ascertained by ^{1}H NMR analysis (Figure S1C, supporting information). The presence of chemical shift signals at 2.24 ppm (*a*) was assigned to the methylidyne protons of alkynyl group, while the signals at 2.59 and 2.70 ppm (*e*) were assigned to the methylene protons groups adjacent to the nitrogen atom, indicating the successful preparation of (PEG$_{45}$(C≡CH))$_7$. The distinctive absorbance peak at about 2098 cm^{-1} in FT-IR spectrum belonging to the alkynyl moieties also conforms the successful preparation of the (PEG$_{45}$(C≡CH))$_7$ (Figure 2B).

The PEG-based hydrogels (Gel-PEG$_n$(N$_3$)$_2$-(PEG$_n$(C≡CH))$_m$) were synthesized by CuAAC of (PEG$_n$(C≡CH))$_m$ and PEG$_n$(N$_3$)$_2$. The gelation was very fast and occurred within 5 min. For comparison, hydrogel of tetrakis (2-propynyloxymethyl) methane (TPOM) and PEG$_{45}$(N$_3$)$_2$ (Gel-TPOM-PEG$_{45}$(N$_3$)$_2$) were also synthesized via CuAAC. Figure 2 D displays FT-IR spectrum of Gel-PEG$_{45}$(N$_3$)$_2$-(PEG$_{45}$(C≡CH))$_7$. The almost disappearance of azido groups at about 2100 cm^{-1} and alkynyl moieties at about 2098 cm^{-1}, confirms the progress of CuAAC between PEG$_n$(N$_3$)$_2$ and (PEG$_n$(C≡CH))$_m$. A series of tough PEG-based hydrogels were prepared from (PEG$_{11}$(C≡CH))$_9$, (PEG$_{11}$(C≡CH))$_{18}$, (PEG$_{11}$(C≡CH))$_{28}$, and (PEG$_{22}$(C≡CH))$_{10}$ macromolecule as the starting materials.

7
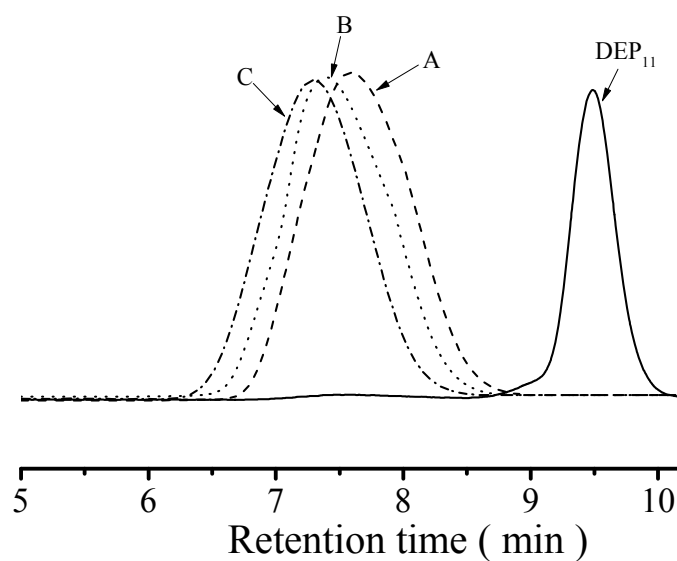
Figure 1. GPC traces of (A) $(PEG_{11}(C\equiv CH))_9$, (B) $(PEG_{11}(C\equiv CH))_{18}$, and (C) $(PEG_{11}(C\equiv CH))_{28}$ using THF as the eluent.
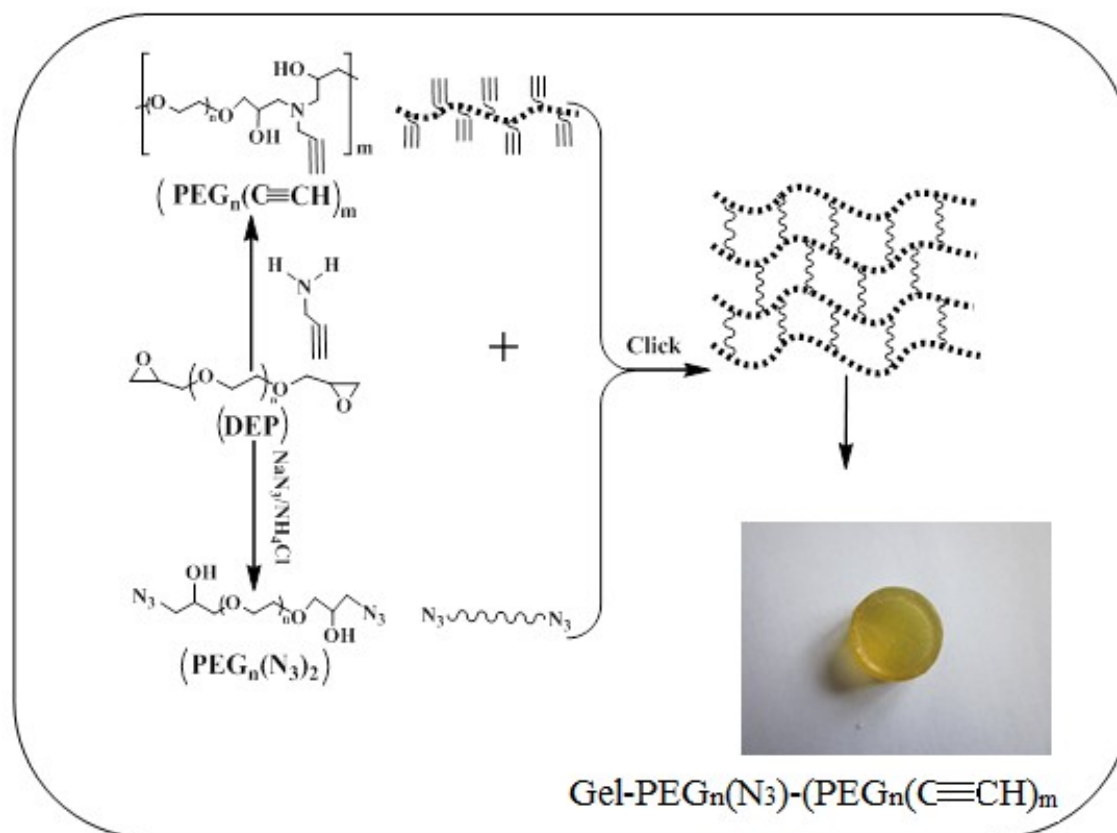
Scheme 1. Synthesis of novel well-defined linear PEG derivatives and preparation of $Gel-PEG_n(N_3)_2-(PEG_n(C\equiv CH))_m$ hydrogels by "Click chemistry".

8
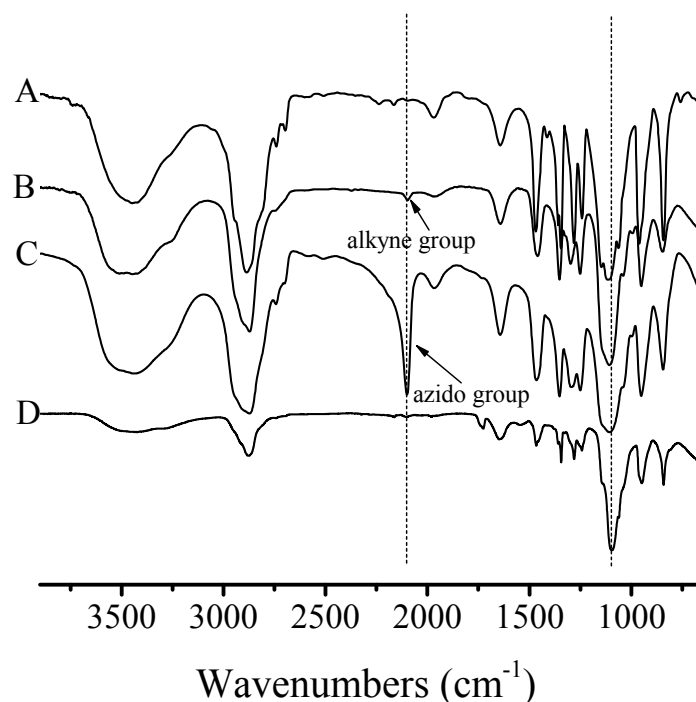
Figure 2. FT-IR spectra of (A) DEP$_{45}$, (B) (PEG$_{45}$(C≡CH))$_7$, (C) PEG$_{45}$(N$_3$)$_7$ and (D) Gel-PEG$_{45}$(N$_3$)$_7$-(PEG$_{45}$(C≡CH))$_7$.

Table 1. Characterization of (PEG$_n$(C≡CH))$_m$

Entry	Polymer sample (PEG$_n$(C≡CH))$_m$	Feed ratio (DEP$_n$:propargylamine)	Number of alkynyl groups (N)	M_n (g·mol^{-1})	M_w (g·mol^{-1})	PDI
				GPC results		
1	(PEG$_{11}$(C≡CH))$_9$	1:1.1	10	4900	8100	1.45
2	(PEG$_{11}$(C≡CH))$_{18}$	1:1.05	19	9300	15100	1.42
3	(PEG$_{11}$(C≡CH))$_{28}$	1:1.02	29	14600	21000	1.38
4	(PEG$_{22}$(C≡CH))$_{10}$	1:1.1	11	10600	15500	1.41
5	(PEG$_{45}$(C≡CH))$_7$	1:1.1	8	14800	22000	1.32

3.2 Physical properties of the PEG-based hydrogels

The effect of cross-linking density and chain lengths of PEG on the swelling ratio (SR) and kinetics of swelling of the PEG-based hydrogels was investigated. Figure 3 shows SR of Gel-PEG$_{11}$(N$_3$)$_2$-(PEG$_{11}$(C≡CH))$_9$, Gel-PEG$_{11}$(N$_3$)$_2$-(PEG$_{11}$(C≡CH))$_{18}$, Gel-PEG$_{11}$(N$_3$)$_2$-(PEG$_{11}$(C≡CH))$_{28}$, Gel-PEG$_{22}$(N$_3$)$_2$-(PEG$_{22}$(C≡CH))$_{10}$, Gel-PEG$_{45}$(N$_3$)$_2$-(PEG$_{45}$(C≡CH))$_7$ and Gel-TPOM-PEG$_{45}$(N$_3$)$_2$ as a function of time. The networks of Gel-PEG$_{11}$(N$_3$)$_2$-(PEG$_{11}$(C≡CH))$_9$,

9

Gel-PEG$_{11}$(N$_3$)$_2$-(PEG$_{11}$(C≡CH))$_{18}$ and Gel-PEG$_{11}$(N$_3$)$_2$-(PEG$_{11}$(C≡CH))$_{28}$ have a same length lattice. However, Gel-PEG$_{11}$(N$_3$)$_2$-(PEG$_{11}$(C≡CH))$_9$ exhibits a SR of about 413% which is higher than those of Gel-PEG$_{11}$(N$_3$)$_2$-(PEG$_{11}$(C≡CH))$_{18}$ (346%) and Gel-PEG$_{11}$(N$_3$)$_2$-(PEG$_{11}$(C≡CH))$_{28}$ (300%). The increase in the number of alkynyl groups in (PEG$_{11}$(C≡CH))$_m$ ((PEG$_{11}$(C≡CH))$_{28}$ > (PEG$_{11}$(C≡CH))$_{18}$ > (PEG$_{11}$(C≡CH))$_9$) could result in more cross-linkings and less molecular defects, or in other words a smaller space volume in the polymer network. Therefore, a higher density of crosslinking points and less defects results in a smaller SR of a hydrogel. Gel-PEG$_{45}$(N$_3$)$_2$-(PEG$_{45}$(C≡CH))$_7$ and Gel-TPOM- PEG$_{45}$(N$_3$)$_2$ have a same length of lattice as PEG$_{45}$ was starting materials for both of them. However, the SR of Gel-PEG$_{45}$(N$_3$)$_2$-(PEG$_{45}$(C≡CH))$_7$ (890%) is smaller than that of Gel-TPOM-PEG$_{45}$(N$_3$)$_2$ (1100%), which suggested that there is less molecular defects in the polymer networks of the former. The SR can be regulated by changing the size of network lattice or the chain length of PEG segments. The SR of Gel-PEG$_{45}$(N$_3$)$_2$-(PEG$_{45}$(C≡CH))$_7$ is higher than that of Gel-PEG$_{22}$(N$_3$)$_2$-(PEG$_{22}$(C≡CH))$_{10}$ and Gel-PEG$_{11}$(N$_3$)$_2$-(PEG$_{11}$(C≡CH))$_9$.
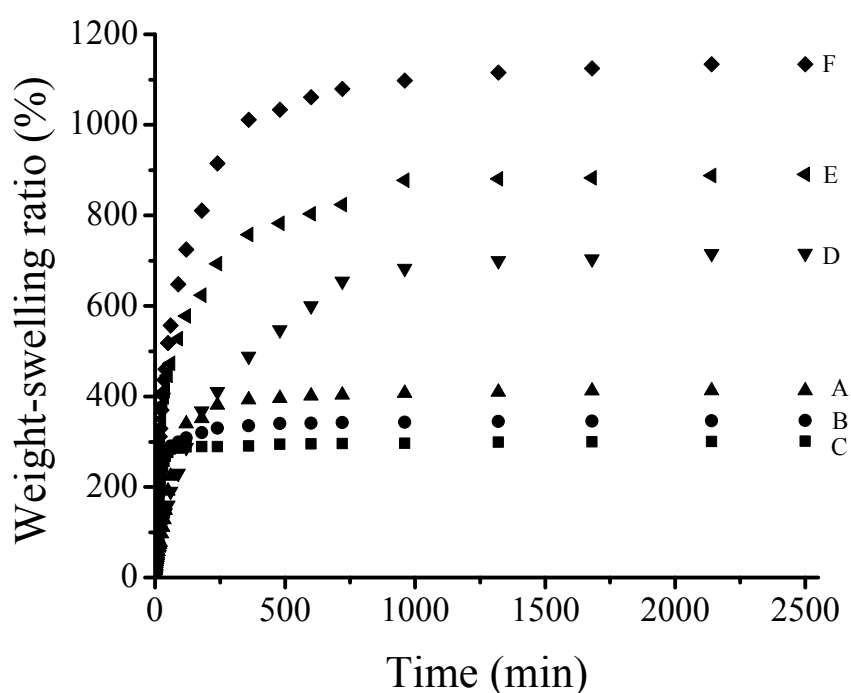
Figure 3. Swelling ratio of (A) Gel-PEG$_{11}$(N$_3$)$_2$-(PEG$_{11}$(C≡CH))$_9$, (B)

Gel-PEG$_{11}$(N$_3$)$_2$-(PEG$_{11}$(C≡CH))$_{18}$,   (C)   Gel-PEG$_{11}$(N$_3$)$_2$-(PEG$_{11}$(C≡CH))$_{28}$,   (D)
Gel-PEG$_{22}$(N$_3$)$_2$-(PEG$_{22}$(C≡CH))$_{10}$,   (E)   Gel-PEG$_{45}$(N$_3$)$_2$-(PEG$_{45}$(C≡CH))$_7$ and   (F)
Gel-TPOM-PEG$_{45}$(N$_3$)$_2$.

Scheme 2 shows a plausible reason for more molecular defects and a larger SR in Gel-TPOM-PEG$_{45}$(N$_3$)$_2$ than in Gel- PEG$_{45}$(N$_3$)$_2$-(PEG$_{45}$(C≡CH))$_7$ as a consequence of difference in the molecular topology structure of PEG polymers. Gel-PEG$_{45}$(N$_3$)$_2$-(PEG$_{45}$(C≡CH))$_7$ and Gel-TPOM-PEG$_{45}$(N$_3$)$_2$ can both have a well-defined molecular structure if the yield of CuAAC reaches 100%. However, the reaction yield never reaches 100%. Hence, broken points or molecular defects exist in the polymer network. With a same reaction yield and a same size of polymer networks for both systems, the number of broken points or the estimated defect ratio (*DR*) in the gel networks of Gel-TPOM-PEG$_n$(N$_3$)$_2$ hydrogel is much higher than that in Gel-PEG$_n$(N$_3$)$_2$-(PEG$_n$(C≡CH))$_m$ system. The DR of Gel-TPOM-PEG$_{45}$(N$_3$)$_2$ and Gel-PEG$_{45}$(N$_3$)$_2$-(PEG$_{45}$(C≡CH))$_7$ can be calculated according to Equation 4 and 5, respectively.

$$DR_{\text{Gel-TPOM-PEG}_n(\text{N}_3)_2} = \frac{T}{4}(1 - Conv_{click}) ; \tag{4}$$

$$DR_{\text{Gel-PEG}_n(\text{N3})2-(\text{PEG}n(\text{C≡CH}))_m} = \frac{T}{m+1}(1 - Conv_{click}) \quad (m \geqslant 8) \tag{5}$$

T: the total amount of cross-linking points; N: the number of alkyl groups.

It can be seen that the number of alkynyl groups in the (PEG$_n$(C≡CH))$_m$ is always bigger than that in TPOM. Hence, under a same reaction yield of CuAAC, $DR_{\text{Gel-PEG}n(\text{N3})2-(\text{PEG}45(\text{C≡CH}))7}$ is smaller than $DR_{\text{Gel-TPOM-PEG}n(\text{N3})2}$. The more broken points and smaller crosslinking functionality in the Gel-TPOM-PEG$_n$(N$_3$)$_2$ lead to the formation of more polymer clusters dissociated from the polymer networks. The dissociation of the polymer clusters from the polymer networks is the core factor that causes the macroscopic molecular defects in the hydrogels. Consequently, the free volume space is created and the mechanical strength of the polymer networks was reduced dramatically. On the contrary, the well-defined molecular structure and higher content of alkynyl groups of (PEG$_n$(C≡CH))$_m$ polymers can largely suppress the formation of macroscopic molecular defects as illustrated in Scheme 2. Therefore, the precise control over molecular topology of polymers is an effective approach to prepare tough hydrogels.

11

Scheme 2. The topology structure of (A) Gel-PEG$_{45}$(N$_3$)$_2$-(PEG$_n$(C≡CH))$_m$ and (B) Gel-TPOM-PEG$_{45}$(N$_3$)$_2$.

The morphology of the PEG-based hydrogels was investigated by SEM. Figure 4 shows the SEM cross-section views of the freeze-dried samples of Gel-PEG$_{11}$(N$_3$)$_2$-(PEG$_{11}$(C≡CH))$_9$, Gel-PEG$_{22}$(N$_3$)$_2$-(PEG$_{22}$(C≡CH))$_{10}$, Gel-PEG$_{45}$(N$_3$)$_2$-(PEG$_{45}$(C≡CH))$_7$ and Gel-TPOM-PEG$_{45}$(N$_3$)$_2$. Almost no pores could be observed in Gel-PEG$_{22}$(N$_3$)$_2$-(PEG$_{22}$(C≡CH))$_{10}$, Gel- PEG$_{45}$(N$_3$)$_2$-(PEG$_{45}$(C≡CH))$_7$ and Gel-PEG$_{11}$(N$_3$)$_2$-(PEG$_{11}$(C≡CH))$_9$ (Figure 4 A-C). However, this is not the case for Gel-TPOM-PEG$_{45}$(N$_3$)$_2$ which has obvious pores in its structure (Figure 4 D). It is possible that the porous structure of a hydrogel is originated from the macroscopic molecular defects of the polymer networks. The denser morphology in Gel-PEG$_{22}$(N$_3$)$_2$-(PEG$_{22}$(C≡CH))$_{10}$, Gel-PEG$_{45}$(N$_3$)$_2$-(PEG$_{45}$(C≡CH))$_7$ and Gel-PEG$_{11}$(N$_3$)$_2$-(PEG$_{11}$(C≡CH))$_9$ further suggests that there are less molecular defects in these hydrogels when compared with Gel-TPOM-PEG$_{45}$(N$_3$)$_2$. SEM results

are in well correlation with those of SR results. It can thus be confirmed that the macroscopic defects of the polymer networks can be significantly suppressed by precise control of molecular topology of the PEG derivatives.
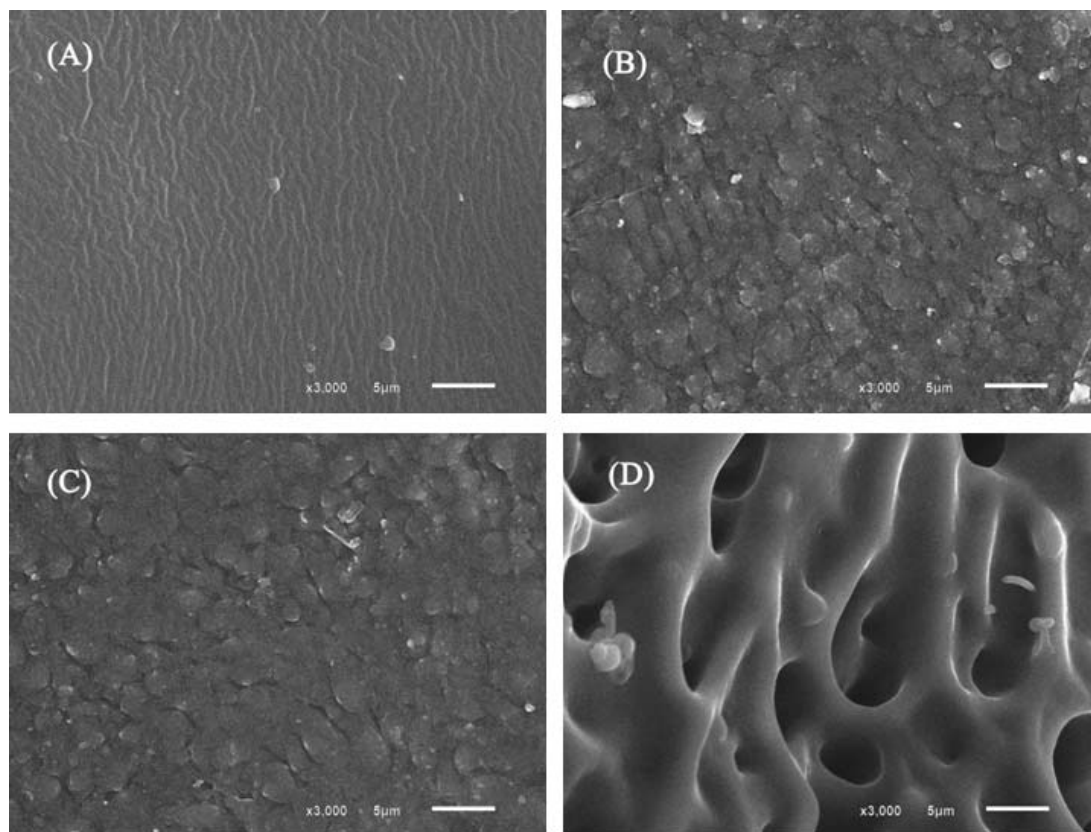
Figure 4. SEM images (cross-section view) of freeze-dried (A) Gel-PEG$_{11}$(N$_3$)$_2$-(PEG$_{11}$(C≡CH))$_9$, (B) Gel-PEG$_{22}$(N$_3$)$_2$-(PEG$_{22}$(C≡CH))$_{10}$, (C) Gel-PEG$_{45}$(N$_3$)$_{25}$-(PEG$_{45}$(C≡CH))$_7$ and (D) Gel-TPOM-PEG$_{45}$(N$_3$)$_2$.

The storage modulus was measured under oscillatory shear conditions to explore the viscoelastic properties of PEG-based hydrogels. Figure 5 demonstrates the storage modulus of Gel-PEG$_{11}$(N$_3$)$_2$-(PEG$_{11}$(C≡CH))$_9$, Gel-PEG$_{11}$(N$_3$)$_2$-(PEG$_{11}$(C≡C$_H$))$_{18}$, Gel-PEG$_{11}$(N$_3$)$_2$-(PEG$_{11}$(C≡CH))$_{28}$, Gel-PEG$_{22}$(N$_3$)$_2$-(PEG$_{22}$(C≡CH))$_{10}$, Gel-PEG$_{45}$(N$_3$)$_2$-(PEG$_{45}$(C≡CH))$_7$ and Gel-TPOM-PEG$_{45}$(N$_3$)$_2$ as a function of frequency. The storage modulus is almost independent of frequency in all cases, indicating that hydrogels were formed prior to recording measurements. The highest storage modulus is achieved by Gel-PEG$_{11}$(N$_3$)$_2$-(PEG$_{11}$(C≡CH))$_{28}$ which is then followed by Gel-PEG$_{11}$(N$_3$)$_2$-(PEG$_{11}$(C≡CH))$_{18}$, Gel-PEG$_{11}$(N$_3$)$_2$-(PEG$_{11}$(C≡CH))$_9$, Gel-PEG$_{22}$(N$_3$)$_2$-(PEG$_{22}$(C≡CH))$_{10}$, Gel-PEG$_{45}$(N$_3$)$_2$-(PEG$_{45}$(C≡CH))$_7$ and Gel-TPOM-PEG$_{45}$(N$_3$)$_2$ in sequence. It is established that the modulus is in proportion

to the cross-linking density. Based on these rheological studies, together with the SEM and SR results, it is appeared that the presence of the highest cross-linking density is in Gel-PEG$_{11}$(N$_3$)$_2$-(PEG$_{11}$(C≡CH))$_{28}$. The cross-linking density decreases with the increase in the chain length of PEG repeating segments (cross-linking density: (PEG$_{11}$(C≡CH))$_m$ > (PEG$_{22}$(C≡CH))$_m$ > (PEG$_{45}$(C≡CH))$_m$; chain length of PEG repeating segments: (PEG$_{11}$(C≡CH))$_m$ < (PEG$_{22}$(C≡CH))$_m$ < (PEG$_{45}$(C≡CH))$_m$), and slightly decreases with the increase in the molecular weight of (PEG$_n$(C≡CH))$_m$ (cross-linking density: (PEG$_{11}$(C≡CH))$_{28}$ > (PEG$_{11}$(C≡CH))$_{18}$ > (PEG$_{11}$(C≡CH))$_9$; molecular weight of (PEG$_n$(C≡CH))$_m$: (PEG$_{11}$(C≡CH))$_{28}$ > (PEG$_{11}$(C≡CH))$_{18}$ > (PEG$_{11}$(C≡CH))$_9$).
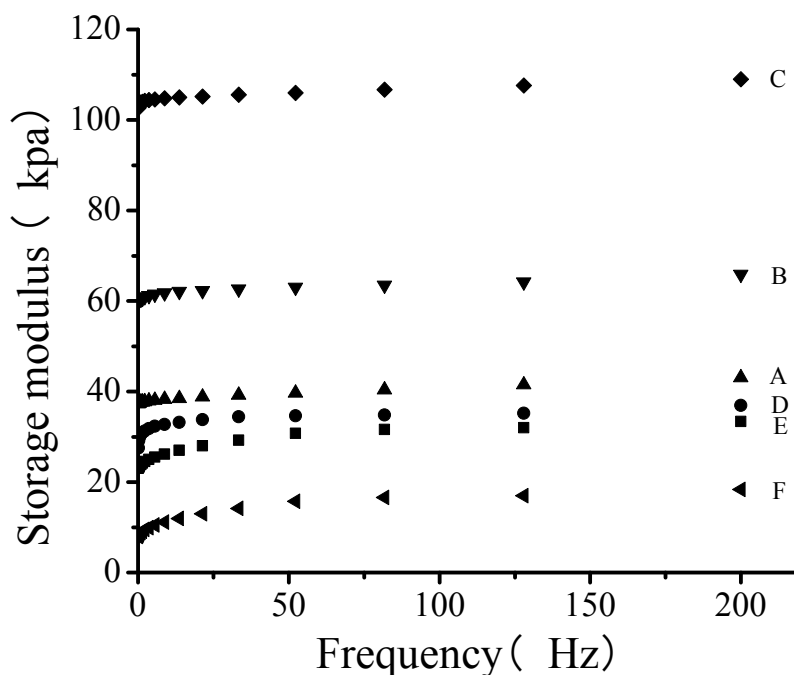
Figure 5. Storage modulus as a function of frequency (Hz) for (A) Gel-PEG$_{11}$(N$_3$)$_2$-(PEG$_{11}$(C≡CH))$_9$, (B) Gel-PEG$_{11}$(N$_3$)$_2$-(PEG$_{11}$(C≡CH))$_{18}$, (C) Gel-PEG$_{11}$(N$_3$)$_2$-(PEG$_{11}$(C≡CH))$_{28}$, (D) Gel-PEG$_{22}$(N$_3$)$_2$-(PEG$_{22}$(C≡CH))$_{10}$, (E) Gel-PEG$_{45}$(N$_3$)$_2$-(PEG$_{45}$(C≡CH))$_7$ and (F) Gel-TPOM-PEG$_{45}$(N$_3$)$_2$. The water contents of hydrogels are about 70%.

Tensile testing of the hydrogels was also characterized. Of note, the mechanical properties of the hydrogels are strongly dependent on the type and the amount of the absorbed solvent as well as the temperature. Thus, all samples with a water content of about 70% were characterized at room temperature. Figure 6 shows the photographic

14

illustration of the tensile testing of Gel-PEG$_{22}$(N$_3$)$_2$-(PEG$_{22}$(C≡CH))$_{10}$. It can be stretched up to 6 times of its original length, and can snap back quickly into the original shape. Gel-PEG$_{11}$(N$_3$)$_2$-(PEG$_{11}$(C≡CH))$_{28}$ has a tensile ratio of about 300%, smaller than 450% of Gel-PEG$_{11}$(N$_3$)$_2$-(PEG$_{11}$(C≡CH))$_9$, 380% of Gel-PEG$_{11}$(N$_3$)$_2$-(PEG$_{11}$(C≡CH))$_{18}$, and 810% of Gel-PEG$_{45}$(N$_3$)$_2$-(PEG$_{45}$(C≡CH))$_7$. These results suggested that the higher the crosslinking density, the smaller the tensile ratio of the polymer networks.

A (original)   B (stretching)   C (restoration)

Figure 6. Stretched changes of Gel-PEG$_{22}$(N$_3$)$_2$-(PEG$_{22}$(C≡CH))$_{10}$.

Gel-PEG$_n$(N$_3$)$_2$-(PEG$_n$(C≡CH))$_m$ also exhibit a very high compressive strength. The illustration of compressive testing of a representative of Gel-PEG$_n$(N$_3$)$_2$-(PEG$_n$(C≡CH))$_m$, Gel-PEG$_{45}$(N$_3$)$_2$-(PEG$_{45}$(C≡CH))$_7$ and Gel-TPOM-PEG$_{45}$(N$_3$)$_2$ are shown and compared in Figure 7. Water content of both samples is about 70 wt.%. As shown in Figure 7, Gel-PEG$_{45}$(N$_3$)$_2$-(PEG$_{45}$(C≡CH))$_7$ can sustain a higher compressive strength than Gel-TPOM-PEG$_{45}$(N$_3$)$_2$. All Gel-PEG$_n$(N$_3$)$_2$-(PEG$_n$(C≡CH))$_m$ remained intact at the maximal load and had similar curves. The typical stress-strain curves of Gel-PEG$_{45}$(N$_3$)$_2$-(PEG$_{45}$(C≡CH))$_7$ and Gel-TPOM-PEG$_{45}$(N$_3$)$_2$ under compression are shown in Figure 8. The maximal compressive strength of Gel-TPOM-PEG$_{45}$(N$_3$)$_2$ is of about 1.28 MPa and it broke at a strain of 40%. As to Gel-PEG$_{45}$(N$_3$)$_2$-(PEG$_{45}$(C≡CH))$_7$, no damage can be observed even at a stress of 62.5 MPa and it can sustain a strain up to 91%. Again, the higher compressive strength of Gel-PEG$_{45}$(N$_3$)$_2$-(PEG$_{45}$(C≡CH))$_7$ can be attributed to the less macroscopic defects in its networks due to the well-defined molecular structure of the (PEG$_{45}$(C≡CH))$_7$.
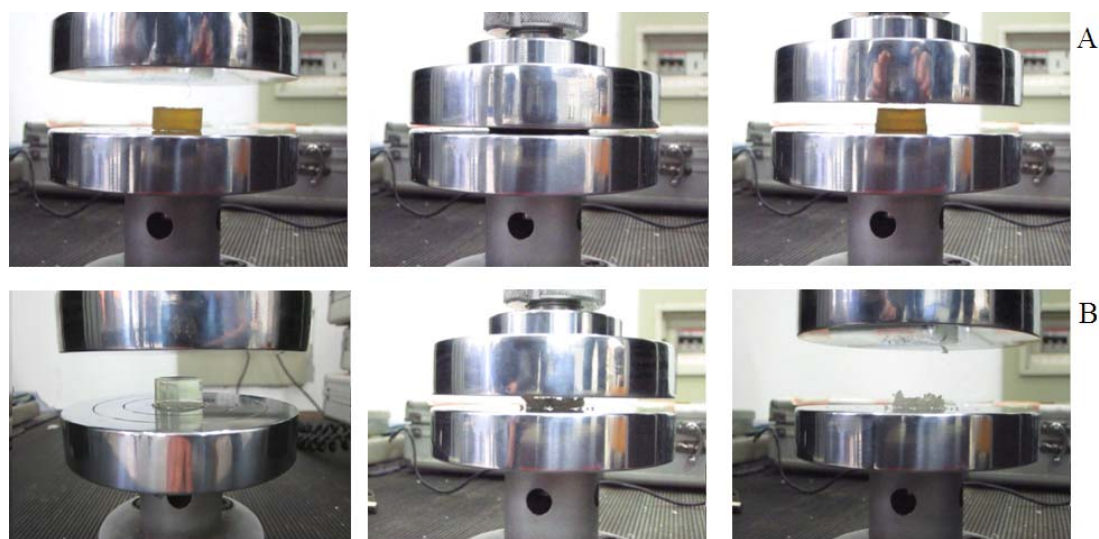
Figure 7. Photographs demonstrating the process of (A) Gel-PEG$_{45}$(N$_3$)$_2$-(PEG$_{45}$(C≡CH))$_7$ and (B) Gel-TPOM-PEG$_{45}$(N$_3$)$_2$ under compression.
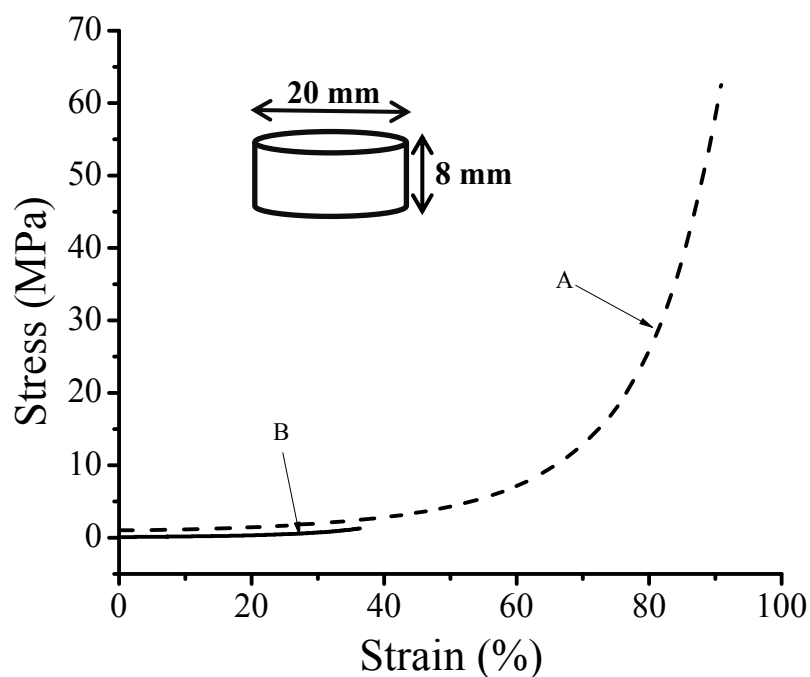
Figure 8. Stress-strain curves for (A) Gel-PEG$_{45}$(N$_3$)$_2$-(PEG$_{45}$(C≡CH))$_7$ and (B) Gel-TPOM-PEG$_{45}$(N$_3$)$_2$ under uniaxial compression.

3.3 Thermal properties

The thermal property of a hydrogel can also reflect its unique characters. The TGA curves of dried Gel-PEG$_{11}$(N$_3$)$_2$-(PEG$_{11}$(C≡CH))$_9$, Gel-PEG$_{11}$(N$_3$)$_2$-(PEG$_{11}$(C≡CH))$_{18}$, Gel-PEG$_{11}$(N$_3$)$_2$-(PEG$_{11}$(C≡CH))$_{28}$, Gel-PEG$_{22}$(N$_3$)$_2$-(PEG$_{22}$(C≡CH))$_{10}$, Gel-PEG$_{45}$(N$_3$)$_2$-(PEG$_{45}$(C≡CH))$_7$ and Gel-TPOM-(PEG$_{45}$(C≡CH))$_7$ are then shown

16

and compared in Figure 9. It can be seen that there was no residue in all cases after thermal decomposition of the PEG-based hydrogels in nitrogen atmosphere. The thermal stability of Gel-PEG$_{11}$(N$_3$)$_2$-(PEG$_{11}$(C≡CH))$_9$, Gel-PEG$_{11}$(N$_3$)$_2$-(PEG$_{11}$(C≡CH))$_{18}$ and Gel-PEG$_{11}$(N$_3$)$_2$-(PEG$_{11}$(C≡CH))$_{28}$ is comparable, but much lower than that of Gel-PEG$_{22}$(N$_3$)$_2$-(PEG$_{22}$(C≡CH))$_{10}$ and Gel-PEG$_{45}$(N$_3$)$_2$-(PEG$_{45}$(C≡CH))$_7$. Gel-PEG$_{11}$(N$_3$)$_2$-(PEG$_{11}$(C≡CH))$_9$, Gel-PEG$_{11}$(N$_3$)$_2$-(PEG$_{11}$(C≡CH))$_{18}$ and Gel-PEG$_{11}$(N$_3$)$_2$-(PEG$_{11}$(C≡CH))$_{28}$ begin to decompose at a close temperature at around 200 °C. Gel-PEG$_{22}$(N$_3$)$_2$-(PEG$_{22}$(C≡CH))$_{10}$ undergoes the thermal decomposition at 260 °C and Gel-PEG$_{45}$(N$_3$)$_2$-(PEG$_{45}$(C≡CH))$_7$ starts to decompose at 302 °C. Gel-TPOM-PEG$_{45}$(N$_3$)$_2$ commences decomposition at around 334 °C. The high contents of hydroxyl groups and C-N bonds in the Gel-PEG$_n$(N$_3$)$_2$-(PEG$_n$(C≡CH))$_m$ structure may account for their relative lower thermal stability when compared with Gel-TPOM-PEG$_{45}$(N$_3$)$_2$ as it was proposed that the higher the content of hydroxyl groups of a hydrogel, the poorer the thermal stability is.[46]
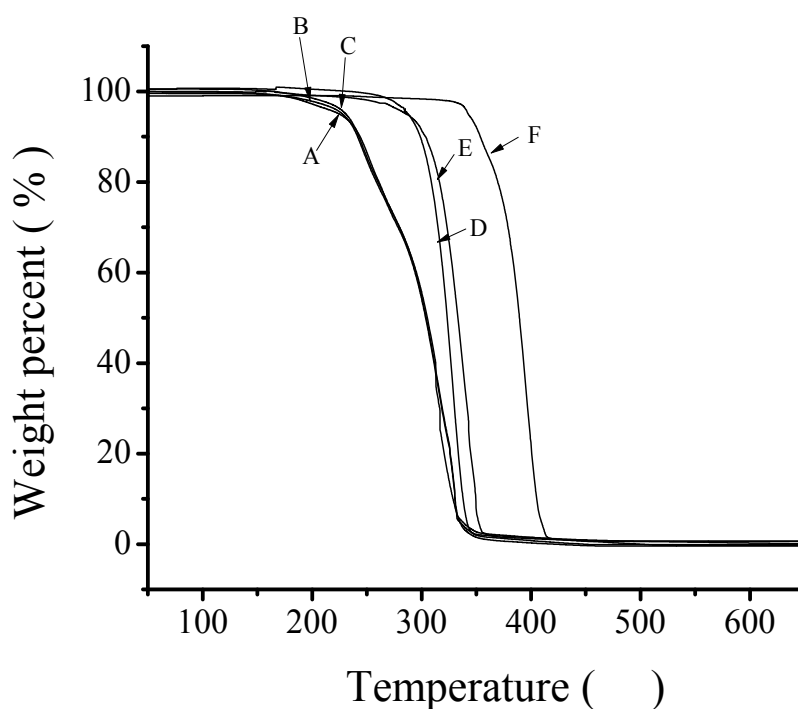
Figure 9. Thermogravimetric analysis (TGA) curves of (A) Gel-PEG$_{11}$(N$_3$)$_2$-(PEG$_{11}$(C≡CH))$_9$, (B) Gel-PEG$_{11}$(N$_3$)$_2$-(PEG$_{11}$(C≡CH))$_{18}$, (C) Gel-PEG$_{11}$(N$_3$)$_2$-(PEG$_{11}$(C≡CH))$_{28}$, (D) Gel-PEG$_{22}$(N$_3$)$_2$-(PEG$_{22}$(C≡CH))$_{10}$, (E) Gel-PEG$_{45}$(N$_3$)$_2$-(PEG$_{45}$(C≡CH))$_7$ and (F) Gel-TPOM-PEG$_{45}$(N$_3$)$_2$.

Figure 10 shows the DSC heating curves of these hydrogels. Gel-PEG$_{22}$(N$_3$)$_2$-(PEG$_{22}$(C≡CH))$_{10}$ exhibits an endothermic peak at 30.84 °C which is the T$_m$ of PEG segments. The T$_m$ of Gel-PEG$_{45}$(N$_3$)$_2$-(PEG$_{45}$(C≡CH))$_7$ is 37.26 °C, higher than that of Gel-PEG$_{22}$(N$_3$)$_2$-(PEG$_{22}$(C≡CH))$_{10}$. This result is consistent with the fact that the higher the molecular weight of polymer chains, the higher the T$_m$ of the polymer networks. The T$_m$ of Gel-TPOM-PEG$_{45}$(N$_3$)$_2$ is 40.67 °C. In comparison to Gel-TPOM-PEG$_{45}$(N$_3$)$_2$, the lower number of macroscopic molecular defects renders Gel-PEG$_{45}$(N$_3$)$_2$-(PEG$_{45}$(C≡CH))$_7$ a well-defined molecular structure which favors the formation of finer crystals, thus accounting for the lower T$_m$ of Gel-PEG$_{45}$(N$_3$)$_2$-(PEG$_{45}$(C≡CH))$_7$. As to Gel-PEG$_{11}$(N$_3$)$_2$-(PEG$_{11}$(C≡CH))$_9$, Gel-PEG$_{11}$(N$_3$)$_2$-(PEG$_{11}$(C≡CH))$_{18}$ and Gel-PEG$_{11}$(N$_3$)$_2$-(PEG$_{11}$(C≡CH))$_{28}$, it is possible that their PEG chain length is too short to be crystallized in the polymer networks. Therefore, no endothermic peaks assigned as T$_m$ can be located for them, but T$_g$ at around -25 °C.
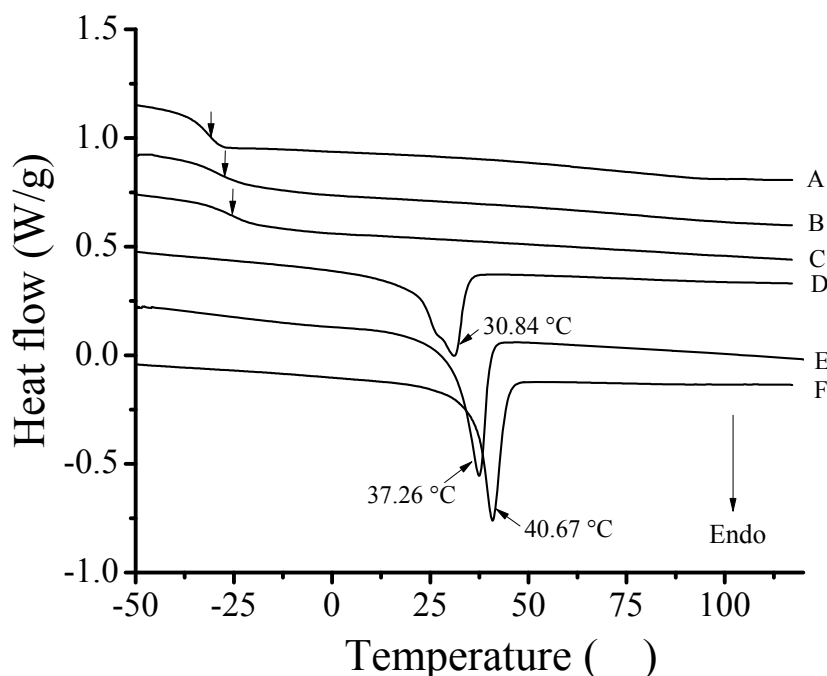
Figure 10. Heating curves of DSC measurements of (A) Gel-PEG$_{11}$(N$_3$)$_2$-(PEG$_{11}$(C≡CH))$_9$, (B) Gel-PEG$_{11}$(N$_3$)$_2$-(PEG$_{11}$(C≡CH))$_{18}$, (C) Gel-PEG$_{11}$(N$_3$)$_2$-(PEG$_{11}$(C≡CH))$_{28}$, (D) Gel-PEG$_{22}$(N$_3$)$_2$-(PEG$_{22}$(C≡CH))$_{10}$, (E) Gel-PEG$_{45}$(N$_3$)$_2$-(PEG$_{45}$(C≡CH))$_7$ and (F) Gel-TPOM-PEG$_{45}$(N$_3$)$_2$.

18

3.4 In vitro degradation

The degradation study was carried out in 0.01M PBS at 37 °C. The weights of PEG-based hydrogels prior to and after being degraded for predetermined time periods were measured and recorded as shown in Figure 11. Interestingly, all PEG-based hydrogels have less than half of their original weights remained except Gel-TPOM-PEG$_{45}$(N$_3$)$_2$ after 10 weeks, indicating that they are degradable under a physiological condition. It can be seen that the degradation rate of Gel-PEG$_{11}$(N$_3$)$_2$-(PEG$_{11}$(C≡CH))$_9$ is remarkably faster than that of Gel-PEG$_{11}$(N$_3$)$_2$-(PEG$_{11}$(C≡CH))$_{18}$. Gel-PEG$_{11}$(N$_3$)$_2$-(PEG$_{11}$(C≡CH))$_{28}$ is degraded at a slower rate than Gel-PEG$_{11}$(N$_3$)$_2$-(PEG$_{11}$(C≡CH))$_{18}$. The difference in the degradation rates may be due to the difference in the cross-linking density in PEG$_{11}$ hydrogels and the difference in relative ratios of C-N and OH bonds over C-O and C-C bonds. The lower the cross-linking density and the higher contents of C-N bonds, the faster the degradation rate. More weight loss was observed in the PEG$_{11}$ hydrogels than in Gel-PEG$_{22}$(N$_3$)$_2$-(PEG$_{22}$(C≡CH))$_{10}$. Moreover, at the end of 10 weeks, Gel-PEG$_{45}$(N$_3$)$_2$-(PEG$_{45}$(C≡CH))$_7$ has about 40% of its initial weight remained, whereas Gel-PEG$_{22}$(N$_3$)$_2$-(PEG$_{22}$(C≡CH))$_{10}$ has about 35% of its initial weight left. It can be seen that the PEG molecular weights could also affect the degradation property of hydrogels.
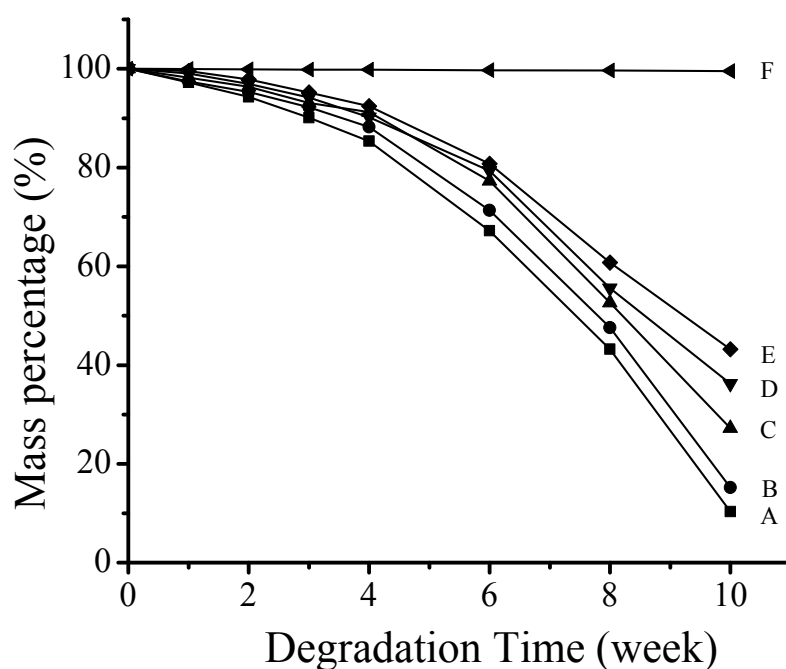
Figure 11. Mass loss profiles of (A) Gel-PEG$_{11}$(N$_3$)$_2$-(PEG$_{11}$(C≡CH))$_9$, (B)

Gel-PEG$_{11}$(N$_3$)$_2$-(PEG$_{11}$(C≡CH))$_{18}$, (C) Gel-PEG$_{11}$(N$_3$)$_2$-(PEG$_{11}$(C≡CH))$_{28}$, (D) Gel-PEG$_{22}$(N$_3$)$_2$-(PEG$_{22}$(C≡CH))$_{10}$, (E) Gel-PEG$_{45}$(N$_3$)$_2$-(PEG$_{45}$(C≡CH))$_7$ and (F) Gel-TPOM-PEG$_{45}$(N$_3$)$_2$ in PBS at 37 °C over time.

3.5 Cell viability assay.

To evaluate the biocompatibility of PEG-based hydrogels, a MTT assay was conducted on L929 cells exposed to the extracts from PEG-based hydrogels. Figure 12 shows the results on MTT assays of Gel-PEG$_{11}$(N$_3$)$_2$-(PEG$_{11}$(C≡CH))$_9$, Gel-PEG$_{11}$(N$_3$)$_2$-(PEG$_{11}$(C≡CH))$_{18}$, Gel-PEG$_{11}$(N$_3$)$_2$-(PEG$_{11}$(C≡CH))$_{28}$, Gel-PEG$_{22}$(N$_3$)$_2$-(PEG$_{22}$(C≡CH))$_{10}$, Gel-PEG$_{45}$(N$_3$)$_2$-(PEG$_{45}$(C≡CH))$_7$ and Gel-TPOM-PEG$_{45}$(N$_3$)$_2$, respectively. Their corresponding results were normalized to that of the positive control at each time point. It is noteworthy that the cell viability with Gel-PEG$_{11}$(N$_3$)$_2$-(PEG$_{11}$(C≡CH))$_9$ reached 96.61%, 95.47%, and 93.16% of that of the positive control after treatment of 24h, 48h and 72h, respectively. Although significant difference could be observed between the cell viability of Gel-PEG$_{11}$(N$_3$)$_2$-(PEG$_{11}$(C≡CH))$_9$ and of the positive control at 24h, 48h, and 72h ($P < 0.05$, at 24h; $P < 0.05$, at 24h; $P < 0.05$, at 72h), respectively, the cell viability with Gel-PEG$_{11}$(N$_3$)$_2$-(PEG$_{11}$(C≡CH))$_9$ could still reach more than 90% of that the positive control even after 72h co-culture. This is also the case for samples of Gel-PEG$_{11}$(N$_3$)$_2$-(PEG$_{11}$(C≡CH))$_{18}$, Gel-PEG$_{11}$(N$_3$)$_2$-(PEG$_{11}$(C≡CH))$_{28}$, Gel-PEG$_{22}$(N$_3$)$_2$-(PEG$_{22}$(C≡CH))$_{10}$, Gel-PEG$_{45}$(N$_3$)$_2$-(PEG$_{45}$(C≡CH))$_7$. In comparison, the cells with the Gel-TPOM-PEG$_{45}$(N$_3$)$_2$ extract only reached around 84% of that of the positive control at 72h ($p < 0.05$). Therefore, the current prepared tough Gel-PEG$_n$(N$_3$)$_2$-(PEG$_n$(C≡CH))$_m$ hydrogels are noncytotoxic and exhibit excellent biocompatibility with L929 cells compared with hydrogels prepared via a traditional method (Gel-TPOM-PEG$_{45}$(N$_3$)$_2$). Future biomedical application of the current tough Gel-PEG$_n$(N$_3$)$_2$-(PEG$_n$(C≡CH))$_m$ hydrogels could thus be desired based on their cytocompatibility.
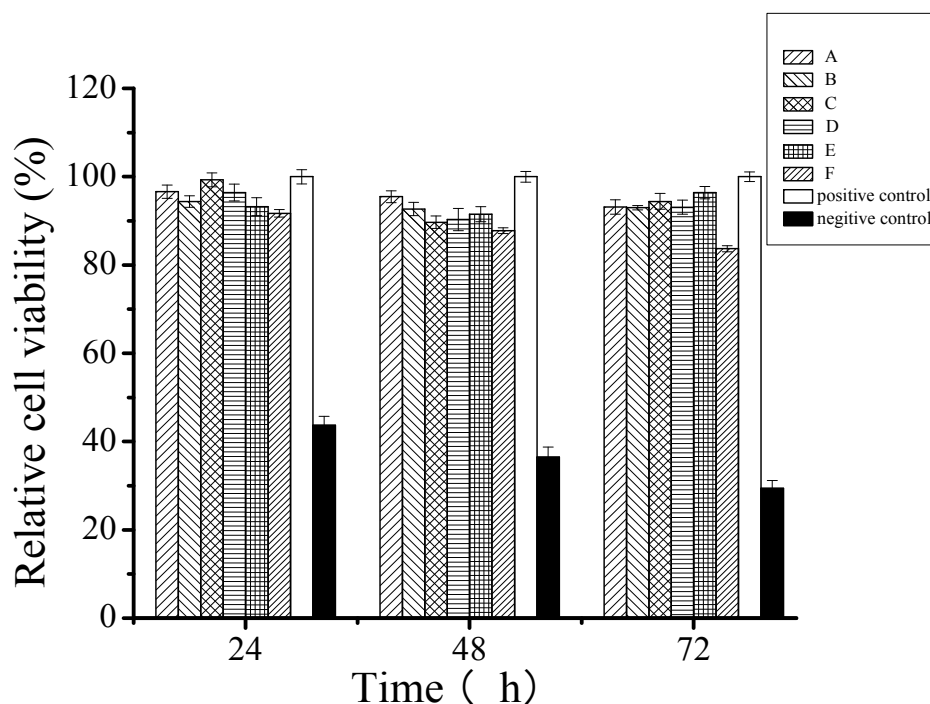
Figure 12. MTT cyctoxicity assay of (A) Gel-PEG$_{11}$(N$_3$)$_2$-(PEG$_{11}$(C≡CH))$_9$, (B) Gel-PEG$_{11}$(N$_3$)$_2$-(PEG$_{11}$(C≡CH))$_{18}$, (C) Gel-PEG$_{11}$(N$_3$)$_2$-(PEG$_{11}$(C≡CH))$_{28}$, (D) Gel-PEG$_{22}$(N$_3$)$_2$-(PEG$_{22}$(C≡CH))$_{10}$, (E) Gel-PEG$_{45}$(N$_3$)$_2$-(PEG$_{45}$(C≡CH))$_7$ and (F) Gel-TPOM-PEG$_{45}$(N$_3$)$_2$ using L929 cell.

4. Conclusion

In this work, PEG-based hydrogels with extremely high strength were successfully prepared via a precise design and control over the molecular topology of the polymeric network. Design and control over the molecular topology can render the polymer network a well-defined molecular structure and a high content of alkynyl groups of (PEG$_n$(C≡CH))$_m$ polymers, further leading to the suppression of forming macroscopic molecular defects. The resulting PEG-based hydrogel materials not only exhibit an excellent and tunable mechanical property, but also have a high degree of swelling, good thermal stability, favorable biodegradability and cytocompatibility. It can be thus ascertained that Gel-PEG$_n$(N$_3$)$_2$-(PEG$_n$(C≡CH))$_m$ has the promising potential as artificial medical devices or scaffolding materials for regenerative medicine.

Acknowledgement

RSC Advances Accepted Manuscript

22

References

1. K. Y. Lee and D. J. Mooney, *Chem. Rev.*, 2001, **101**, 1869-1879.
2. K. T. Nguyen and J. L. West, *Biomaterials*, 2002, **23**, 4307-4314.
3. J. L. Drury, R. G. Dennis and D. J. Mooney, *Biomaterials*, 2004, **25**, 3187-3199.
4. J. L. Drury and D. J. Mooney, *Biomaterials*, 2003, **24**, 4337-4351.
5. R. Langer and D. A. Tirrell, *Nature*, 2004, **428**, 487-492.
6. S. X. Lu and K. S. Anseth, *Macromolecules*, 2000, **33**, 2509-2515.
7. B. D. Yang, Y. C. Lu and G. S. Luo, *Industrial & Engineering Chemistry Research*, 2012, **51**, 9016-9022.
8. F. Yao, X. X. Ji, B. P. Lin and G. D. Fu, in *Multi-Functional Materials and Structures Engineering, Icmmse 2011*, ed. J. Tian, 2011, vol. 304, pp. 131-134.
9. A. J. Kerin, A. Coleman, M. R. Wisnom and M. A. Adams, *Clinical Biomechanics*, 2003, **18**, 960-968.
10. J. P. Gong and Y. Osada, in *High Solid Dispersions*, ed. M. Cloitre, 2010, vol. 236, pp. 203-246.
11. H. Gao, N. Wang, X. F. Hu, W. J. Nan, Y. J. Han and W. G. Liu, *Macromol. Rapid Commun.*, 2013, **34**, 63-68.
12. J. L. Zhang, N. Wang, W. G. Liu, X. L. Zhao and W. Lu, *Soft Matter*, 2013, **9**, 6331-6337.
13. L. Tang, W. G. Liu and G. P. Liu, *Adv. Mater.*, 2010, **22**, 2652-+.
14. J. Yang, C. R. Han, J. F. Duan, F. Xu and R. C. Sun, *Acs Applied Materials & Interfaces*, 2013, **5**, 3199-3207.
15. B. Xu, H. J. Li, Y. Y. Wang, G. Z. Zhang and Q. S. Zhang, *Rsc Advances*, 2013, **3**, 7233-7236.
16. T. Huang, *Applied Physics a-Materials Science & Processing*, 2012, **107**, 905-909.
17. Y. Wang and D. J. Chen, *J. Colloid Interface Sci.*, 2012, **372**, 245-251.
18. A. F. Zhu, G. Li and J. M. Jiang, *Journal of Macromolecular Science Part B-Physics*, 2012, **51**, 1002-1010.
19. T. Sakai, T. Matsunaga, Y. Yamamoto, C. Ito, R. Yoshida, S. Suzuki, N. Sasaki, M. Shibayama and U. I. Chung, *Macromolecules*, 2008, **41**, 5379-5384.
20. M. Fukasawa, T. Sakai, U. I. Chung and K. Haraguchi, *Macromolecules*, 2010, **43**, 4370-4378.
21. T. Nakajima, H. Furukawa, J. P. Gong, E. K. Lin and W. L. Wu, in *Polymer Networks: Synthesis, Properties, Theory and Applications*, ed. C. S. Patrickios, 2010, vol. 291-292, pp. 122-126.
22. H. Furukawa and J. P. Gong, in *Artificial Muscle Actuators Using Electroactive Polymers*, eds. P. Vincenzini, Y. BarCohen and F. Carpi, 2009, vol. 61, pp. 40-45.
23. T. Tominaga, Y. Osada and J. P. Gong, in *Chemomechanical Instabilities in Responsive Materials*, eds. P. Borckmans, P. DeKepper, A. R. Khokhlov and S. Metens, 2009, pp. 117-138.
24. W. Yang, H. Furukawa and J. P. Gong, *Adv. Mater.*, 2008, **20**, 4499-4503.
25. H. J. Kwon, Y. Osada and J. P. Gong, *Polym. J.*, 2006, **38**, 1211-1219.
26. J. P. Gong, Y. Katsuyama, T. Kurokawa and Y. Osada, *Adv. Mater.*, 2003, **15**, 1155-+.
27. M. C. Darnell, J. Y. Sun, M. Mehta, C. Johnson, P. R. Arany, Z. G. Suo and D. J. Mooney, *Biomaterials*, 2013, **34**, 8042-8048.
28. J. Kopecek, *Journal of Polymer Science Part a-Polymer Chemistry*, 2009, **47**, 5929-5946.
29. J. D. Kretlow and A. G. Mikos, *Tissue Eng.*, 2007, **13**, 927-938.

30. X. H. Liu, J. M. Holzwarth and P. X. Ma, *Macromolecular Bioscience*, 2012, **12**, 911-919.

31. E. S. Place, J. H. George, C. K. Williams and M. M. Stevens, *Chem. Soc. Rev.*, 2009, **38**, 1139-1151.

32. M. Malkoch, R. Vestberg, N. Gupta, L. Mespouille, P. Dubois, A. F. Mason, J. L. Hedrick, Q. Liao, C. W. Frank, K. Kingsbury and C. J. Hawker, *Chem. Commun.*, 2006, 2774-2776.

33. H. M. N. El-Din and A. W. M. El-Naggar, *Designed Monomers and Polymers*, 2014, **17**, 322-333.

34. L. Garber, C. Chen, K. V. Kilchrist, C. Bounds, J. A. Pojman and D. Hayes, *Journal of Biomedical Materials Research Part A*, 2013, **101**, 3531-3541.

35. X. Y. Hu, J. Wang and H. H. Huang, *Cellulose*, 2013, **20**, 2923-2933.

36. J. M. Page, A. J. Harmata and S. A. Guelcher, *Journal of Biomedical Materials Research Part A*, 2013, **101**, 3630-3645.

37. C. Demitri, A. Sannino, F. Conversano, S. Casciaro, A. Distante and A. Maffezzoli, *Journal of Biomedical Materials Research Part B-Applied Biomaterials*, 2008, **87B**, 338-345.

38. G. Mapili, Y. Lu, S. C. Chen and K. Roy, *Journal of Biomedical Materials Research Part B-Applied Biomaterials*, 2005, **75B**, 414-424.

39. J. M. Zhu and R. E. Marchant, *Expert Review of Medical Devices*, 2011, **8**, 607-626.

40. Y. Yuan, A. K. Zhang, J. Ling, L. H. Yin, Y. Chen and G. D. Fu, *Soft Matter*, 2013, **9**, 6309-6318.

41. L. Q. Xu, F. Yao, G. D. Fu and E. T. Kang, *Biomacromolecules*, 2010, **11**, 1810-1817.

42. H. E. Colley, V. Hearnden, K. Wayakanon, D. Cecchin, S. Armes, G. Battaglia, C. Murdoch and M. H. Thornhill, *Oral Diseases*, 2012, **18**, 7-7.

43. K. Haraguchi and T. Takehisa, *Adv. Mater.*, 2002, **14**, 1120-1124.

44. A. Saha, S. De, M. C. Stuparu and A. Khan, *J. Am. Chem. Soc.*, 2012, **134**, 17291-17297.

45. G. D. Fu, H. Jiang, F. Yao, L. Q. Xu, J. Ling and E. T. Kang, *Macromol. Rapid Commun.*, 2012, **33**, 1523-1527.